PAPER

Using molecular rotors to probe gelation†

Jaclyn Raeburn,[a] Lin Chen,[a] Salmah Awhida,[a] Robert C. Deller,[b] Manu Vatish,[c] Matthew I. Gibson[b] and Dave J. Adams*[a]

A series of fluorescent probes, including a number of molecular rotors, have been used to follow the self-assembly of dipeptide-based low molecular weight gelators. We show that these probes can be used to gain an insight into the assembly process. Thioflavin T, a commonly used stain for β-sheets, appears to act as a molecular rotor in these gelling systems, with the fluorescence data closely matching that of other rotors. The molecular rotor was incorporated into an assay system with glucose oxidase to enable glucose-concentration specific gelation and hence generating a fluorescent output. Applying this system to urine from patients with various levels of glycosuria (a symptom of diabetes), it was found to provide excellent correlation with different clinical assessments of diabetes. This demonstrates a new concept in gelation-linked biosensing for a real clinical problem.

Introduction

Several classes of low molecular weight gelator (LMWG) form hydrogels that are tunable by altering the parameters that trigger gelation.[1–4] Along with changes in the self-assembly trigger,[5] the introduction of additives[6–12] and salts[13–16] can have an influence on the final behaviour and attributes of the gel. Even subtle changes in the gelation conditions can affect the final gel properties.[5] Despite knowing that tunability of the final properties of these materials is possible, the process by which these gels form is not always well understood. If the self-assembly process could be better understood, there is the possibility to specifically tune materials to possess desired properties for a specific application.

When a gel forms, the LMWG in solution must firstly self-assemble, usually triggered by a change in solution conditions, before the assembled fibrils continue to grow, entangle and form a network capable entrapping the solvent and affording a gel.[1,17] This increase in structure in solution ultimately leads to an increase in viscosity as the transition from a solution to a gel occurs.

Fluorescent probes have been frequently used to monitor the formation and/or presence of micellar structures.[18] For example, pyrene exhibits changes in fluorescence intensity and emission wavelength when going from an aqueous environment to the interior of a hydrophobic micelle.[19] The fluorescent data can be interpreted to give an indication of the critical micelle concentration of the material. Similar studies have been carried out with the dye 8-anilino-1-naphthalenesulfonic acid (ANS), which is also sensitive to hydrophobic environments associated with micelles. For example, ANS has been used to probe the micelle production by amino acid amphiphile gelators.[20]

In recent years, a class of fluorescent materials known as molecular rotors has been used as non-mechanical viscosity sensors in some bio- and polymeric materials.[21–26] These materials differ from fluorescent probes such as pyrene and ANS as they are sensitive to changes in viscosity and therefore sensitive to structural changes within close proximity to the rotor structure itself. Fluorescent molecular rotors are flexible molecules which undergo an intramolecular twisting motion upon photo-excitation.[27] This twisting leads to a return to the ground state of the molecule *via* non-radiative emission or by red-shifted emission (dependent on molecular structure). The fluorescence quantum yield is therefore dependent on local viscosity.[21]

Molecular rotors have become increasingly popular due to their high sensitivity and ability to compare the results to mechanical data collected using rheology.[22] Rheological data provides information regarding the evolution of structure during the assembly and hydrogelation process. Molecular rotors have the potential to provide information that can correlate with this rheological data.[22] Perhaps the most commonly studied molecular rotor is 9-(2,2-dicyanovinyl)julolidine (DCVJ). DCVJ has been shown to be particularly sensitive in a variety of solvents,[28] in organized assemblies,[29] and in polymer solutions and solid matrices.[22,30,31] For example, Loutfy and Teegarden demonstrated an increase in fluorescent intensity of DCVJ was dependent on tacticity of PMMA.[32]

A common probe for peptide assembly and folding is Thioflavin T (ThT). ThT is widely used as a stain for β-amyloid

[a] *Department of Chemistry, University of Liverpool, Crown Street, Liverpool, L69 7ZD, UK. E-mail: d.j.adams@liverpool.ac.uk*

[b] *Department of Chemistry, University of Warwick, Coventry, CV4 7AL, UK*

[c] *Nuffield Department of Obstetrics & Gynaecology, University of Oxford, Oxford, UK*

structures[23,24,33–38] and has also been used to demonstrate aggregation of oligopeptides.[39,40] It has also been suggested that ThT is a molecular rotor.[41] The fluorescent intensity of ThT increases in the presence of glycerol–water mixtures with increasing viscosity.[27,41] It has been hypothesised that ThT binds to β-amyloid structures but the increase in fluorescence intensity is determined by the rigidity of the local environment in which ThT is located *i.e.* the local viscosity affects the ability of the benzathiole ring to rotate relative to the aminobenzene ring in the excited state.[41] We have previously used ThT to follow the gelation profile of a dipeptide-based LMWG.[42,43] Liang *et al.* have used Congo red, another stain for amyloid fibres to probe assembly of dipeptide and tripeptide LMWG.[44] Here, we compare the use of ThT and two molecular rotors, DCVJ and 9-(2-carboxy-2-cyanovinyl)julolidine (CCVJ) with a hydrophobic dye (Nile blue) to probe the self-assembly of dipeptide-based LMWG. We show that these probes can be used to gain an insight into the assembly process. To demonstrate the potential of the gelators as a pro-fluorescence biosensors, we use a mixed LMWG–ThT system to detect glucose in the urine of diabetic patients and benchmark against a currently used clinical grading system.

Results and discussion

The LMWG used in this study are shown in Fig. 1, along with the structures for ThT, DCVJ, CCVJ[21] and Nile blue. **1** and **2** form gels using a change in pH. The self-assembly of **1** has not been previously reported, but we have previously detailed the assembly of **2** in detail.[42] For both **1** and **2**, a transparent solution is formed a concentration of 5 mg mL^{-1} at pH 10. When the pH is lowered below the pK_a of the LMWG, a gel is formed.[45] To adjust the pH, we use the hydrolysis of glucono-δ-lactone (GdL) to gluconic acid.[42,45–47] This method allows for a slow, homogeneous pH change, which is ideal to follow the process of self-assembly.

Following the pH during the gelation process of **1** (Fig. 2b), it can seen that the pH decreases to a plateau value, which correlates with the apparent pK_a of the terminal carboxylic acid of the LMWG.[45,48] When this pK_a is reached, gelation begins as can be seen from the rheological data (Fig. 2c). The storage modulus (G′) gradually increases as the pH evolves, following a two-stage that we have observed a number of times previously.[42,46,49] We have interpreted this two-stage self-assembly process in the
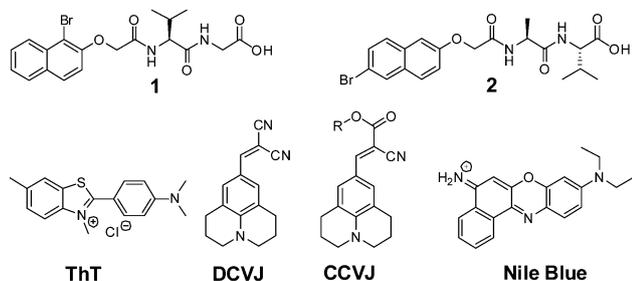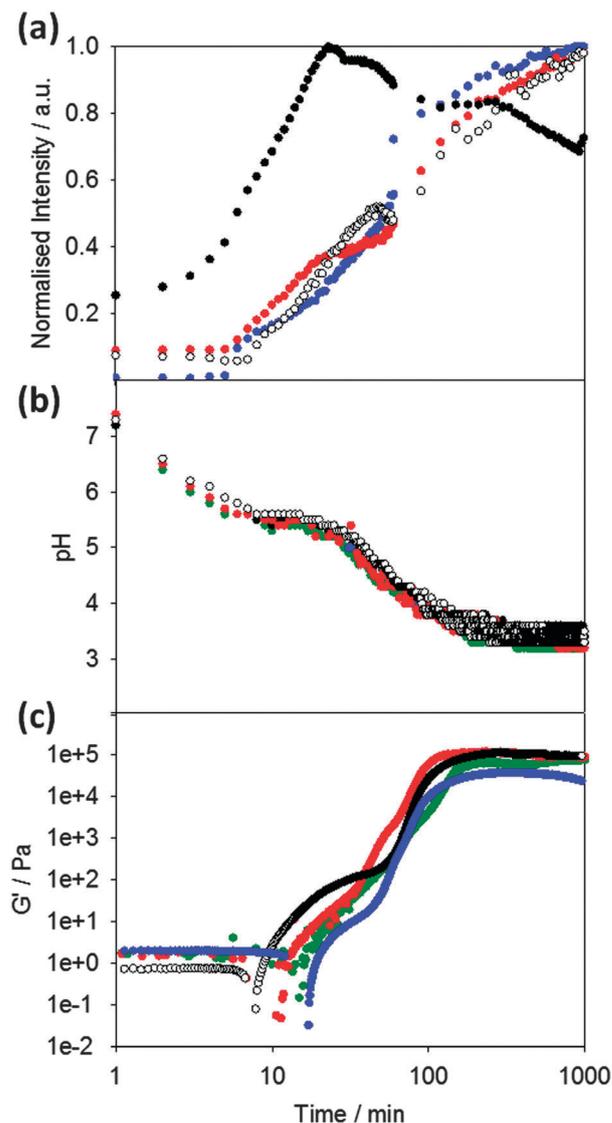

Fig. 2 Kinetics of gelation of **1**. (a) Normalised changes in fluorescence of the dyes: Thioflavin T (blue data) at 475 nm (λ_{ex} = 455 nm); DCVJ (red), at 485 nm (λ_{ex} = 470 nm), CCVJ (open circles) at 485 nm (λ_{ex} = 460 nm), and Nile blue (black) at 660 nm (λ_{ex} = 630 nm) upon addition of a solution of **1** solutions to GdL (8 mg mL^{-1}). (b) Changes in pH with time after addition of a solution of **1** to GdL (8 mg mL^{-1}) (green data) and in the presence of ThT (blue), DCVJ (red) and Nile blue (black). (c) Rheological properties during the kinetic process of gelation of **1** (green data) and in the presence of ThT (blue), DCVJ (red) and Nile blue (black).

Fig. 1 The structures of LMWG **1** and **2**, as well as ThT, DCVJ, CCVJ (R = (CH$_2$CH$_2$O)OCH$_3$), and Nile blue.

rheological behavior as being due to the formation of uniformly charged fibres at the pK_a of the LMWG with little initial association.[42,49] When the charge density is lowered, the fibres become sufficiently hydrophobic for lateral association and entanglement of the fibres to occur. There are subtle differences in the rheological data in the presence of the different dyes, which we discuss below.

To probe the kinetics of gelation *via* spectroscopic methods, a fluorescent probe was added to the LMWG solution before gelation occurred. The presence of these molecular rotors in the gelling solution allows the kinetic process to be probed (Fig. 2a).

Here, we compare the data obtained with ThT (which as noted above has the potential to act as a stain for β-sheet formation or as a molecular rotor), to that obtained with the known rotor DCVJ. We also compare these data to that obtained on addition of Nile blue, a hydrophobic stain. We use Nile blue because although it stains the fibres of such gelators,[46] it is not a molecular rotor. It is important to note that despite the known instability of ThT at high pH,[50] adding ThT immediately prior to GdL or alternatively adding GdL immediately prior to the addition of ThT was sufficient to allow ThT fluorescence to be monitored during the gelation process.

On adding the fluorescence dyes, the kinetics of the pH change induced by the addition of GdL is unaffected by the presence of either molecular rotor or Nile blue (Fig. 2b). The apparent pK_a of the LMWG in solution is also unaffected as shown by the similarity in the plateau during the pH change. Hence, the presence of the dyes does not seem to significantly affect the kinetics of the gelation (Fig. 2b). However, the bulk rheological data shows slight differences, with the data for ThT showing a slightly slower onset of gelation than when other dyes are incorporated. This is of course a bulk measurement and so may not represent the local molecular assembly (see below for further discussion).

The fluorescence data for ThT closely mirrors that for the known rotor DCVJ (Fig. 2a). The data follows a two-stage process. No fluorescence is observed until the pH drops to the pK_a of 1 at about 6–8 minutes. At this point, the fluorescence intensity steadily increases before subtly undergoing a sharper increase in intensity (at a pH ∼ 5.2) leading to a plateau in intensity around pH 3.6. This data implies that ThT and DCVJ co-assemble with the structures of 1 in the same manner during the assembly process. There are subtle differences in the rate of fluorescence increase, but the profiles are very similar. It has been suggested that ThT can influence and even accelerate fibril formation in some amyloid systems.[51] The similarity in fluorescence data here for the different rotors suggests that this is not happening here, although it is possible that the small differences in rheological timescales may be due to these effects. The similarity in profile for the fluorescence data from both ThT and DCVJ compared to the rheological data can be seen from Fig. 2b and c.

Nile blue shows a different behavior to that of ThT and DCVJ. The fluorescence intensity increases shortly before the pK_a of 1 is reached, but there is a sharp increase in intensity before a short plateau, and then another sharp increase. The emission intensity then reaches a plateau at pH 5.0, before decreasing gradually. We interpret this as the formation of sufficiently hydrophobic structures at the pK_a to co-assemble with the Nile blue. Indeed at this point, there is a shift in the emission maximum of the fluorescence (Fig. S1, ESI†). The second increase in fluorescence also occurs at relatively early times and we suggest that Nile blue is sensitive to subtle structural/morphological changes that are occurring, presumably from spherical micelles to more elongated fibrous structures, in line with our previously structural studies.[42] After the formation of long fibres, further structural evolution does not significantly change the local hydrophobicity and hence the plateau in
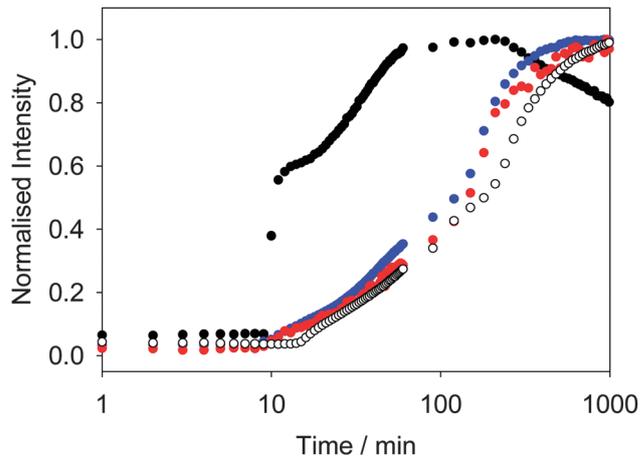

Fig. 3 Normalised changes in fluorescence of the dyes: Thioflavin T (blue data) at 475 nm (λ_{ex} = 455 nm); DCVJ (red) at 485 nm (λ_{ex} = 470 nm); CCVJ (open circles) at 485 nm (λ_{ex} = 460 nm) and Nile blue (black) at 660 nm (λ_{ex} = 630 nm) upon addition of solutions of 2 to GdL (8 mg mL^{-1}).

fluorescence for Nile blue at pH 5.0. The intensity decreases as lower pH values are reached; this is due to the sensitivity of Nile blue to changes in pH.[52]

Similar behavior is observed for other LMWG. We have previously described in detail the assembly process for 2.[42] At high pH, spherical micellar structures are formed.[14] On lowering the pH, the self-assembly occurs by a two-stage process, which again begins at the pK_a of 2. As above, the two-stage process could be followed rheologically and by monitoring the fluorescence of ThT added into the system.[42] Concentrating on the fluorescence data, the fluorescence data for ThT is again similar to that of DCVJ (Fig. 3). Interestingly, the profile of the fluorescence intensity from a more hydrophilic rotor, CCVJ, is also extremely similar. As for 1, the profile with Nile blue is very different to that from the rotors (Fig. 3).

Hence, whilst the fluorescence behavior for ThT closely mirrors that of the known rotors, it is very different to a simple hydrophobic probe. For both 1 and 2, we interpret the changes in fluorescence of the rotors to the local viscosity, but the changes in fluorescence of Nile blue as being due to changes in local hydrophobicity. A combination of dyes therefore allows us to probe different structural changes. The rotors can be used to probe the structural evolution post fibre assembly, but it also appears that the Nile blue data is pointing to subtle structural re-organisation at the pK_a of the gelator. Such re-organisation must be occurring as the original spherical structures become fibres. Since the data for ThT and DCVJ follows the same two-stage process, presumably the increase in fluorescence initially is due to incorporation of the dye within the fibres. However, these are relatively flexible and hence the local viscosity is relatively low. On removal of the charge from the growing fibres and subsequent entanglement and lateral association, the local viscosity increases again before reaching a plateau.

Whilst we can use the probes to follow the self-assembly process, correlation of the absolute fluorescence with the rheological data is less clear. In many ways, this is unsurprising

since the fluorescence data must be probing the local molecular environment around the dye, whilst the rheological data measures the bulk properties at a significantly longer length-scale. As can be seen from Fig. 2c, whilst the timescale for structural evolution is similar in the presence of all rotors (Fig. 2a and b), the absolute rheological data differ. The rheological data for the gel formed with ThT lags behind that for the other dyes. We interpret this as follows: whilst similar fibrous structures are formed in all cases (as is shown by SEM, Fig. 4), the overall network is affected by the co-packing. This may be due to changes in the rate of growth of the fibres. The final rheological data for the gels also differ. We attribute this to both the differences in fibre growth and/or the propensity for the fibres to entangle for example. For dyes such as CCVJ, which contain a relatively hydrophilic moiety, it may be that the incorporation of the dye leads to a change in the hydrophilicity of the fibre surface and so affects the lateral packing of the fibres. This may explain the slightly retarded switch on of the second stage of assembly observed in Fig. 3 compared to the data for DCVJ. We therefore expect that this approach will be able to inform re the primary self-assembled structures, but there will potentially be differences at longer length scales. Nonetheless, it is interesting that the fluorescence data with the different rotors matches the two stage process for the rheology, implying that, at least to some degree, both the molecular assembly and the assembly of the fibres is captured by the rotors.

We are able to use the rotors in the presence of the LMWG to prepare sensors. There are a number of reports detailing the use of LMWG as sensors. Typically, the formation of a gel is used as the detection criteria. The drawback here is that the gelation is generally determined by visual (potentially subjective) determination of the point of lack of flow on inversion or tipping of the vial. For LMWG, mechanical agitation can affect the assembly process and so can lead to artefacts. As proof of principle, we examined the detection of glucose, which is an important from the perspective of diabetes. Gelation-based sensors for glucose have been reported. Xu et al. have shown that a dipeptide-based LMWG can be used;[53] glucose oxidase is incorporated within the gelator solution. Glucose oxidase converts glucose to gluconic acid. This leads to a reduction in pH and hence gelation. This was determined by the formation or dissolution of a gel.[53] Similarly, Liu et al. have used pectin in the presence of calcium carbonate, with gelation occurring as the decrease in pH results in the dissolution of the calcium carbonate and hence cross-linking of the pectin chains.[54] We hypothesized that we could use the fluorescence from an incorporated rotor as the means of sensing, and hence we would not need to determine the ability of the sample to flow.

On the basis of the above data, we utilized LMWG **2**, since the pK_a is slightly higher. We incorporated glucose oxidase into a solution of **2** at pH 10.7, along with ThT. On the basis of initial screening, a concentration of **1** of 2.5 mg mL^{-1} was used. Example data from a screen carried out using a high through-put plate, incorporating different amounts of glucose are shown in Fig. 5. Eight repeats (A–H) of the same solutions are shown, monitoring the kinetics over two hours. Decreasing amounts of glucose were added in columns 1 to 11, with column 12 showing data for the addition of pure water.

As can been seen from Fig. 5, there is no signal until a critical value of glucose is reached. Between 0.74 and 2.2 mg mL^{-1}, an increase in fluorescence is seen to a plateau, whereas data for 3.1 mg mL^{-1} and above show the evolution of a second increase in fluorescence after this plateau. Full pH data for samples where different amounts of glucose were added are shown in Fig. S2 (ESI†). Monitoring absolute fluorescence intensity for solutions with a range of added glucose showed again that there was a very low intensity until a critical concentration of glucose was reached. The intensity then increased linearly with glucose concentration until 1.9 mg mL^{-1} of glucose, where a plateau was reached.

Following this proof-of-principle study, we wanted to test this in a real clinical context. Glucose being present in urine is used as a marker for diabetes, but any biosensor must be able to function in the presence of various levels of salts, urea and protein which are also present. The ability to diagnose disease from urine is particularly appealing from a clinical perspective (e.g. compared to blood) but the variability of its solute composition presents a barrier.
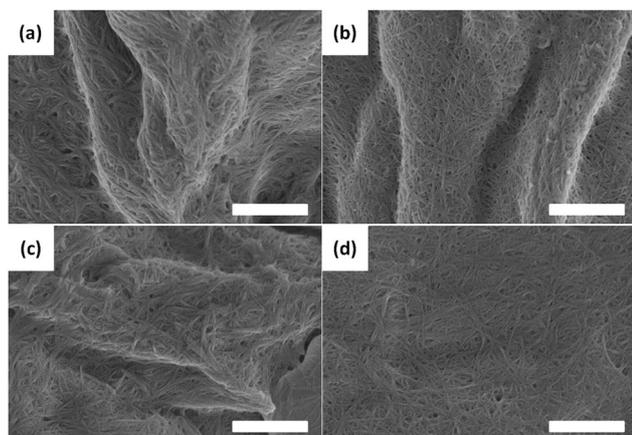

Fig. 4 SEM images of the fibres formed on gelation of **1** alone (a), or in the presence of (b) Nile blue; (c) ThT; (d) DCVJ. In all cases, the scale bar represents 1 μm.
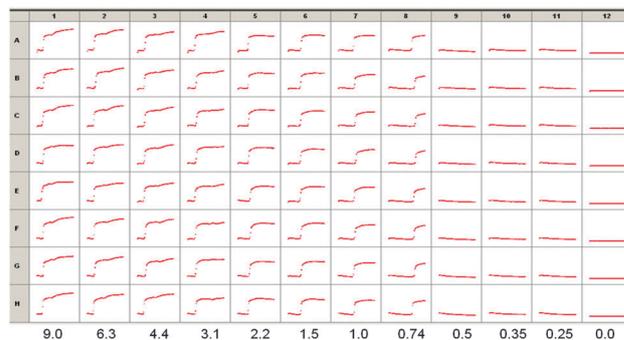

Fig. 5 High throughput fluorescence screen for eight repeat samples (rows A–H). Different amounts of glucose were added, shown underneath each column in mg mL^{-1}. The excitation wavelength was 440 nm, and the emission wavelength 485 nm. Data is shown over 2 hours; longer times lead to errors due to evaporation from the cells.
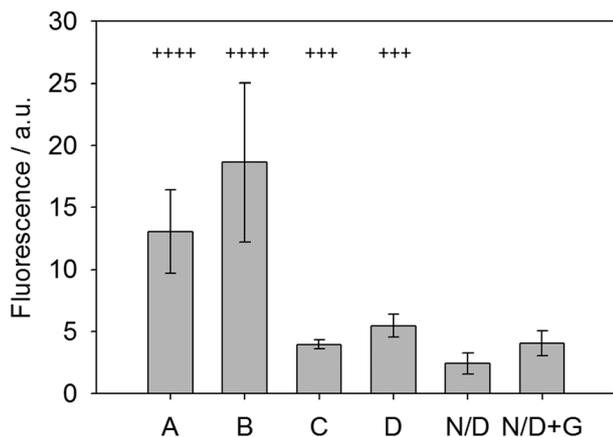
Fig. 6 Fluorescence signal (485 nm) obtained using ThT in the presence of **2** on addition to urine after 30 minutes. The error bars represent the standard deviation from 3 repeats. Samples A and B assessed as 4+; C and D assessed as 3+ by dipsticks. N/D = non-diabetic. N/D + G = non-diabetic urine doped with glucose.

To test this new system, fresh urine was collected from patients in the morning following fasting and the glucose levels (indicative of glycosuria) were assessed using standard urine dipsticks. These dipsticks give possible scores of Nil (absent), 1+ (250 mg L^{-1}), 2+ (500 mg L^{-1}), 3+ (1000 mg L^{-1}) and 4+ (2000 mg L^{-1}). These urine samples were then used with the LMWG, ThT and glucose oxidase system and the fluorescence measured after allowing the gel to form over 30 minutes. Fig. 6 shows the results of this analysis. Samples labeled as N/D were non-diabetic without any glucose (dipstick scores of 2+ or 1+) and showed very little signal. When doped with 5 mg mL^{-1} glucose (N/D + G, Fig. 6), the sample showed a small but significant increase in fluorescence, demonstrating the sensing concept. Two other clinical samples, C and D, were used and graded as 3+ (using dipsticks). Both of these samples gave significant increase in fluorescence, again relative to the non-diabetic samples. Finally, clinical sample A and B (with 4+ scores) gave significant fluorescence enhancement relative to all the others. Samples A/B and C/D did not give identical values as the dipstick grading system covers a range of glucose levels, whereas our system shows a broader spectrum of responses due to the variations in glucose levels between patients. Crucially, this data suggests that is possible to discriminate between unhealthy levels of glycosuria (3+) from lower levels (2+ and 1+) using a simple fluorescence output. In particular, the lack of signal at low concentrations is a useful tool to prevent false positives. This proof of concept data shows that such a gelation-triggered fluorescence biosensor could be used as an alternative on/off sensory system for glycosylurea or even adapted for other urine-based biosensing.

Conclusions

In conclusion, different fluorescent probes can be used to follow the assembly of dipeptide-based gelators. Here, using GdL and hence obtaining a slow pH change allows this process to be reproducibly followed with time. ThT seems to act as a molecular rotor, with the data closely following that of DCVJ.

Nile blue however acts as a hydrophobic stain and utilising different dyes allows us to better understand the assembly process. There are clearly a number of structural re-organisations taking place, which are probed in different ways by the different dyes.

An important point is that the absolute rheological values are not correlated with the fluorescent output. This can be understood by the dyes presumably affecting to some degree the rate of growth of the fibres or potentially the hydrophobicity of the fibres, which will then affect the propensity of the fibres to crosslink. Whilst beyond the scope of this study, this potentially implies that it may be possible to induce changes in the nucleation of the fibres, which may allow more tunable gels to be formed.

We can use a combination of dye and gelator to provide a sensitive sensor. This exploits the fluorescence changes with pH. Similar gelators have been used to form sensors for glucose, but rely on the ability to invert the vial (*i.e.* gelation with certain rheological properties) as the output, which is open to interpretation by the observer. The combination of dye and gelator allows us to discriminate between different urine samples of clinical relevance.

Experimental

Materials

ThT, DCVJ and Nile blue were purchased from Sigma Aldrich and used as received. CCVJ was synthesized according to a literature procedure.[21] Gelator **1** was synthesized from 1-bromo-2-naphthol, following the synthetic protocols described previously.[42] Gelator **2** was synthesized as described previously.[42]

***tert*-Butyl-2-(1-bromonaphthalen-2-yloxy)acetate.** ^{1}H NMR (CDCl$_3$): 8.10 (d, ArH, 1H, $^3J_{HH}$ = 11.7 Hz), 7.71 (d, ArH, 1H, $^3J_{HH}$ = 9.3 Hz), 7.52 (t, ArH, 1H, $^3J_{HH}$ = 8.1 Hz), 7.35 (t, ArH, 1H, $^3J_{HH}$ = 8.1 Hz), 7.12 (d, ArH, 1H, $^3J_{HH}$ = 9.3 Hz), 4.68 (s, OCH$_2$C=O, 2H), 1.45 ppm (s, OC(CH$_3$)$_3$, 9H). ^{13}C NMR (CDCl$_3$): 167.6, 152.5, 133.1, 130.2, 128.8, 128.0, 127.8, 126.4, 124.7, 114.8, 109.8, 82.5, 67.3, 41.9, 28.0, 27.7 ppm. MS: ES$^+$: accurate mass calculated: 359.0267 found 359.0259 ([M + Na]$^+$).

2-(1-Bromonaphthalen-2-yloxy)acetic acid. ^{1}H NMR (d$_6$-DMSO): 8.10 (s, ArH, 1H,), 7.96 (d, ArH, 1H, $^3J_{HH}$ = 9.0 Hz), 7.93 (d, ArH, 1H, $^3J_{HH}$ = 9.1 Hz), 7.63 (dd, ArH, 1H, $^3J_{HH}$ = 8.2 Hz), 7.46 (d, ArH, 1H, $^3J_{HH}$ = 9.1 Hz), 7.40 (d, ArH, 1H), 4.97 (s, OCH$_2$C=O, 2H), 13.7 (s, OH) ppm. ^{13}C NMR (d$_6$-DMSO): 170.3, 152.7, 132.6, 129.8, 129.4, 128.6, 128.5, 125.6, 124.8, 115.0, 107.6, 65.9 ppm. Accurate mass calculated: 278.9657. Found 278.9662 ([M–H]$^-$).

Methyl-2-(2-((1-bromonaphthalen-2-yl)oxy)acetamido)-3-methyl-butanoate. ^{1}H NMR (CDCl$_3$): 8.22 (d, ArH, 1H, $^3J_{HH}$ = 8.9), 7.85 (d, ArH, 1H, $^3J_{HH}$ = 8.9), 7.81 (d, ArH, 1H, $^3J_{HH}$ = 8.3), 7.61 (t, ArH, 1H, $^3J_{HH}$ = 6.4), 7.45 (t, ArH, 1H, $^3J_{HH}$ = 7.2), 7.20 (d, ArH, 1H, $^3J_{HH}$ = 8.9), 4.71 (s, OCH$_2$C=O, 2H), 4.67 (q, NHCHCH(CH$_3$)$_2$, 1H, $^3J_{HH}$ = 5.9), 3.76 (s, OCH$_3$, 3H), 2.29 (m, (CH$_3$)$_2$CH, 1H) 1.01 (d, (CH$_3$)$_2$CH, 3H, $^3J_{HH}$ = 6.7), 0.99 (d, (CH$_3$)$_2$CH, 3H, $^3J_{HH}$ = 6.7) ppm. ^{13}C NMR (CDCl$_3$): 171.7, 167.5, 151.4, 132.9, 130.4, 129.4, 128.2, 128.1, 126.2, 125.0, 114.3, 109.6, 68.6, 56.8, 52.2, 31.2, 19.0, 17.7 ppm. Mass calculated: 416.0473 found 416.0486 ([M + Na]$^+$).

2-(2-((1-Bromonaphthalen-2-yl)oxy)acetamido)-3-methylbutanoic acid. ^{1}H NMR (d_6-DMSO): 8.10 (d, ArH, 1H, $^3J_{HH}$ = 8.5 Hz), 8.20 (d, NH, 1H, $^3J_{HH}$ = 8.6 Hz), 7.98 (d, ArH, 1H, $^3J_{HH}$ = 9.0 Hz), 7.94 (d, ArH, 1H, $^3J_{HH}$ = 10.1 Hz), 7.65 (t, ArH, 1H, $^3J_{HH}$ = 8.5 Hz), 7.48 (t, ArH, 1H, $^3J_{HH}$ = 7.7 Hz), 7.44 (d, ArH, H, $^3J_{HH}$ = 9.0 Hz), 4.89 (d, OCH$_2$C=O, 2H, $^3J_{HH}$ = 5.6 Hz), 4.29 (m, NHCHCH(CH$_3$)$_2$), 2.15 (m, (CH$_3$)$_2$CH, 1H), 0.91 (m, (CH$_3$)$_2$CH, 6H) ppm. ^{13}C NMR (d_6-DMSO): 172.9, 167.7, 152.5, 132.5, 130.0, 129.7, 129.6, 128.7, 125.6, 125.0, 115.5, 107.8, 68.1, 57.0, 30.4, 19.4, 18.0 ppm. Accurate mass calculated: 402.0317 found 402.0331 ([M–H]$^-$).

Ethyl-2-(2-(2-((1-bromonaphthalen-2-yl)oxy)acetamido)-3-methyl-butanamido)acetate. ^{1}H NMR (CDCl$_3$): 8.23 (d, NH, 1H, $^3J_{HH}$ = 8.8 Hz), 7.82 (dd, ArH, 2H, $^3J_{HH}$ = 7.8, 4.9 Hz), 7.62 (m, ArH, 2H), 7.45 (t, ArH, 1H, $^3J_{HH}$ = 4.6 Hz), 7.20 (d, ArH, 1H, $^3J_{HH}$ = 8.8 Hz), 6.54 (s, NH, 1H), 4.72 (s, OCH$_2$C=O, 2H), 4.44 (dd, NHCHCH(CH$_3$)$_2$, 1H, $^3J_{HH}$ = 6.2, 3.8 Hz), 4.07 (dd, NHCH$_2$C=O, 2H, $^3J_{HH}$ = 6.9, 5.5 Hz), 3.76 (s, OCH$_3$, 2H), 2.32 (m, (CH$_3$)$_2$CH, 1H), 1.05 (d, OCH$_2$CH$_3$, 3H, $^3J_{HH}$ = 7.1 Hz), 0.97 (m, (CH$_3$)$_2$CH, 6H) ppm. ^{13}C NMR (CDCl$_3$): 171.2, 170.5, 168.4, 151.7, 133.3, 130.8, 129.9, 128.6, 128.5, 126.7, 125.5, 114.8, 110.2, 69.0, 58.5, 52.9, 41.6, 31.2, 19.7, 18.3 ppm. Accurate mass calculate: 473.0692 found 473.0688 ([M + Na]$^+$).

2-(2-(2-((1-Bromonaphthalen-2-yl)oxy)acetamido)-3-methyl-butanamido)acetic acid. ^{1}H NMR (d_6-DMSO): 8.90 (t, NH, 1H, $^3J_{HH}$ = 7.3 Hz), 8.53 (d, ArH, 1H, $^3J_{HH}$ = 8.1 Hz), 8.42 (d, ArH, 1H, $^3J_{HH}$ = 8.8 Hz), 8.38 (d, ArH, 1H, $^3J_{HH}$ = 8.6 Hz), 8.32 (d, ArH, 1H, $^3J_{HH}$ = 8.6 Hz), 8.08 (t, NH, 1H, $^3J_{HH}$ = 7.8 Hz), 7.90 (m, ArH, 2H), 5.29 (d, OCH$_2$C=O, 2H, $^3J_{HH}$ = 8.1 Hz), 4.78 (dd, NHCHCH(CH$_3$)$_2$, 1H, $^3J_{HH}$ = 5.6, 3.2 Hz), 4.21 (dd, NHCH$_2$C=O, 2H, $^3J_{HH}$ = 6.4, 4.0 Hz), 2.48 (m, (CH$_3$)$_2$CH, 1H), 1.33 (d, (CH$_3$)$_2$CH, 6H, $^3J_{HH}$ = 6.7 Hz), 1.30 (d, (CH$_3$)$_2$CH, 6H, $^3J_{HH}$ = 6.7 Hz) ppm. ^{13}C NMR (d_6-DMSO): 171.5, 171.2, 167.4, 152.5, 132.5, 130.0, 129.7, 128.7, 128.6, 125.6, 125.0, 115.5, 107.8, 68.2, 57.1, 31.4, 19.5, 17.9 ppm. Accurate mass calculated: 459.0536 found 459.0532 ([M + Na]$^+$).

Hydrogel preparation

A 0.5 wt% stock solution of dipeptide material at approximately pH 10–11 was prepared by adding dilute sodium hydroxide solution (1 molar equivalent of a 0.1 M solution) with stirring until fully dissolved. The gelator stock solution was added to a weighed amount of GdL and gently swirled to dissolve GdL. The sample was then left to stand to allow gelation to occur over several hours.

Fluorescence

Fluorescence spectra were obtained on a PerkinElmer Luminescence spectrometer LS55. Gels were formed *in situ* as described above in 1.0 cm path-length PMMA cuvettes. Emission spectra were recorded with a scan rate of 100 nm min^{-1}, with sequential scans every minute for one hour and then every 30 min for ~18 hours at 25 °C. For each of the dyes tested, the following parameters were used: 100 µL of 5 µM dye per 2 mL of gelator solution for Thioflavin T, DCVJ and CCVJ; 40 µL of 0.1 µM Nile blue per 2 mL of gelator solution.

Rheology

Rheological measurements were carried out using an Anton Paar Physica MCR101 rheometer using a parallel plates geometry. Time sweep measurements were performed at a constant frequency of 10 rad s^{-1} and a strain of 0.5% at 25 °C. G' and G'' were measured over time for ~20 hours. A 25 mm sandblasted plate was used for **1** and a 50 mm sandblasted plate was used for **2** to minimise slippage.

pH measurements

A calibrated FC200 pH probe (HANNA instruments) with a (6 mm × 10 mm) conical tip was used for the pH measurements and pK_a titrations. The stated accuracy of the pH measurements is ±0.1. Kinetic pH measurements during gelation were taken by monitoring the pH *in situ* and by taking pH measurements every 60 s for ~18 hours at 25 °C.

Scanning electron microscopy

SEM images were recorded using a Hitachi S-4800 FE-SEM at 3 keV. A portion of the hydrogels was placed on a glass cover slip attached to a sticky carbon tab. The hydrogel was air-dried directly on the coverslip. The samples were gold coated for 3 minutes at 15 mA using a sputter coater (EMITECH K550X) prior to imaging.

High throughput screening of the gelation of 2

A 96-well plate fluorescence instrument (Bioteck, Synergy HT Multi-detection plate reader) was used. The concentrations of stock solution used in the measurements were 5 mg mL^{-1} for **2**, 25 mg mL^{-1} for glucose oxidise (GoX) and 50 µM for ThT, respectively. To prepare 100 µL testing solutions in each well, 50 µL of the stock solution of **2** were dispensed first (apart from the wells in column 12 which were filled with pure water as a blank), followed by adding appropriate volumes of glucose stock solution and extra water into each well to make up different glucose concentrations and a total volume of 100 µL. The glucose concentration decreased from column 1 to column 11 with a dilution factor of 0.7. The final concentrations of glucose in column 1 were 9 mg mL^{-1} and that of **2** in each well was 2.5 mg mL^{-1} at starting pH 10.7. All the transferring and diluting of the solutions in the wells were performed by robotic dispensing instrument (Eppendorf epMotion 5075PC). To monitor the early stage of the gelation process in the first 2 hours by fluorescence, 1.3 µL of ThT stock solution was added into each of the solutions. The excitation filter used for fluorescence was 440 ± 30 nm and emission was monitored at 485 ± 20 nm. As soon as the 1 µL of GoX was added into each column on the plate, the kinetic reading of fluorescence was start immediately and the intensity of ThT emission at 485/20 with time collected.

Urine samples

Urine samples were taken with written informed consent (Research Ethics Approval 05/Q2802/122, Coventry and Warwick Research Ethics Committee). Patients with clinical glycosuria were identified using standard urine glucose dipsticks (Roche Diagnostics),

which grade glycosuria as Nil (absent), 1+ (250 mg dL^{-1}), 2+ (500 mg dL^{-1}), 3+ (1000 mg dL^{-1}) and 4+ (2000 mg dL^{-1}) on urine samples taken in the morning (fasting) and collected midstream in a clean sterile container. Glycosuria occurs when the capacity of the kidney to absorb glucose is exceeded by high circulating levels of glucose and is almost invariably associated with diabetes mellitus.

Fluorescence assay with urine samples

Measurements were performed for each patient (2 × 4+, 2 × 3+ and 1 × Nil) in triplicate using the following methodology: 50 µL of 0.5 wt% solution of **2** was added to 100 µL urine in a 96 well plate followed by 1.5 µL 10 µM ThT. To initiate the reaction, 1.0 µL of 25 mg mL^{-1} glucose oxidase was added and the samples mixed by gentle pipetting prior to incubation at room temperature for a period of 30 minutes enabling gelation. The fluorescence of ThT attributed to the changing hydrophobic environment was measured using a Synergy HT Multi-mode plater reader (BioTek Ltd, Bedfordshire, UK) with excitation at 440/30 nm and emission at 485/20 nm with the values reported representing the mean and error bars ± standard deviation.

Acknowledgements

Notes and references

1 P. Terech and R. G. Weiss, *Chem. Rev.*, 1997, **97**, 3133–3160.
2 R. G. Weiss, *J. Am. Chem. Soc.*, 2014, **136**, 7519–7530.
3 S. Fleming and R. V. Ulijn, *Chem. Soc. Rev.*, 2014, **43**, 8150–8177.
4 N. Zweep and J. H. van Esch, *Functional Molecular Gels*, The Royal Society of Chemistry, 2014, pp. 1–29.
5 J. Raeburn, A. Zamith Cardoso and D. J. Adams, *Chem. Soc. Rev.*, 2013, **42**, 5143–5156.
6 D. Li, H. Wang, D. Kong and Z. Yang, *Nanoscale*, 2012, **4**, 3047–3049.
7 J. Wang, Z. Wang, J. Gao, L. Wang, Z. Yang, D. Kong and Z. Yang, *J. Mater. Chem.*, 2009, **19**, 7892–7896.
8 L. E. Buerkle and S. J. Rowan, *Chem. Soc. Rev.*, 2012, **41**, 6089–6102.
9 L. Chen, S. Revel, K. Morris, D. G. Spiller, L. C. Serpell and D. J. Adams, *Chem. Commun.*, 2010, **46**, 6738–6740.
10 G. Pont, L. Chen, D. G. Spiller and D. J. Adams, *Soft Matter*, 2012, **8**, 7797–7802.
11 E. Carretti, S. Grassi, M. Cossalter, I. Natali, G. Caminati, R. G. Weiss, P. Baglioni and L. Dei, *Langmuir*, 2009, **25**, 8656–8662.
12 Y. J. Adhia, T. H. Schloemer, M. T. Perez and A. J. McNeil, *Soft Matter*, 2012, **8**, 430–434.
13 S. Roy, N. Javid, J. Sefcik, P. J. Halling and R. V. Ulijn, *Langmuir*, 2012, **28**, 16664–16670.
14 L. Chen, G. Pont, K. Morris, G. Lotze, A. Squires, L. C. Serpell and D. J. Adams, *Chem. Commun.*, 2011, **47**, 12071–12073.
15 B. Ozbas, K. Rajagopal, L. Haines-Butterick, J. P. Schneider and D. J. Pochan, *J. Phys. Chem. B*, 2007, **111**, 13901–13908.
16 V. J. Nebot, J. J. Ojeda-Flores, J. Smets, S. Fernández-Prieto, B. Escuder and J. F. Miravet, *Chem. – Eur. J.*, 2014, **20**, 14465–14472.
17 L. A. Estroff and A. D. Hamilton, *Chem. Rev.*, 2004, **104**, 1201–1218.
18 M. da Graça Miguel, *Adv. Colloid Interface Sci.*, 2001, **89–90**, 1–23.
19 K. Kalyanasundaram and J. K. Thomas, *J. Am. Chem. Soc.*, 1977, **99**, 2039–2044.
20 D. Das, A. Dasgupta, S. Roy, R. N. Mitra, S. Debnath and P. K. Das, *Chem. – Eur. J.*, 2006, **12**, 5068–5074.
21 M. A. Haidekker, T. P. Brady, S. H. Chalian, W. Akers, D. Lichlyter and E. A. Theodorakis, *Bioorg. Chem.*, 2004, **32**, 274–289.
22 M. A. Haidekker and E. A. Theodorakis, *Org. Biomol. Chem.*, 2007, **5**, 1669–1678.
23 A. Hawe, M. Sutter and W. Jiskoot, *Pharm. Res.*, 2008, **25**, 1487–1499.
24 M. Lindgren and P. Hammarström, *FEBS J.*, 2010, **277**, 1380–1388.
25 F. Attanasio, C. Bonaccorso, F. Bellia, S. Cataldo, C. G. Fortuna, G. Musumarra, B. Pignataro and E. Rizzarelli, *Eur. J. Org. Chem.*, 2013, 3635–3639.
26 M. L. Viriot, M. C. Carré, C. Geoffroy-Chapotot, A. Brembilla, S. Muller and J. F. Stoltz, *Clin. Hemorheol. Microcirc.*, 1998, **19**, 151–160.
27 N. Amdursky, Y. Erez and D. Huppert, *Acc. Chem. Res.*, 2012, **45**, 1548–1557.
28 K. Y. Law, *Chem. Phys. Lett.*, 1980, **75**, 545–549.
29 M. A. Haidekker, T. Ling, M. Anglo, H. Y. Stevens, J. A. Frangos and E. A. Theodorakis, *Chem. Biol.*, 2001, **8**, 123–131.
30 A. Benjelloun, A. Brembilla, P. Lochon, M. Adibnejad, M.-L. Viriot and M.-C. Carré, *Polymer*, 1996, **37**, 879–883.
31 D. Zhu, M. A. Haidekker, J.-S. Lee, Y.-Y. Won and J. C. M. Lee, *Macromolecules*, 2007, **40**, 7730–7732.
32 R. O. Loutfy and D. M. Teegarden, *Macromolecules*, 1983, **16**, 452–456.
33 M. Groenning, L. Olsen, M. van de Weert, J. M. Flink, S. Frokjaer and F. S. Jørgensen, *J. Struct. Biol.*, 2007, **158**, 358–369.
34 M. R. H. Krebs, E. H. C. Bromley and A. M. Donald, *J. Struct. Biol.*, 2005, **149**, 30–37.
35 S. Freire, M. H. de Araujo, W. Al-Soufi and M. Novo, *Dyes Pigm.*, 2014, **110**, 97–105.
36 H. Levine, *Protein Sci.*, 1993, **2**, 404–410.
37 M. Biancalana, K. Makabe, A. Koide and S. Koide, *J. Mol. Biol.*, 2009, **385**, 1052–1063.
38 R. Sabate, L. Rodriguez-Santiago, M. Sodupe, S. J. Saupe and S. Ventura, *Chem. Commun.*, 2013, **49**, 5745–5747.
39 M. Tena-Solsona, J. F. Miravet and B. Escuder, *Chem. – Eur. J.*, 2014, **20**, 1023–1031.

40 U. Anand and M. Mukherjee, *Langmuir*, 2013, **29**, 2713–2721.

41 V. I. Stsiapura, A. A. Maskevich, V. A. Kuzmitsky, V. N. Uversky, I. M. Kuznetsova and K. K. Turoverov, *J. Phys. Chem. B*, 2008, **112**, 15893–15902.

42 L. Chen, K. Morris, A. Laybourn, D. Elias, M. R. Hicks, A. Rodger, L. Serpell and D. J. Adams, *Langmuir*, 2010, **26**, 5232–5242.

43 S. Grigoriou, E. K. Johnson, L. Chen, D. J. Adams, T. D. James and P. J. Cameron, *Soft Matter*, 2012, **8**, 6788–6791.

44 G. Liang, K. Xu, L. Li, L. Wang, Y. Kuang, Z. Yang and B. Xu, *Chem. Commun.*, 2007, 4096–4098.

45 L. Chen, S. Revel, K. Morris, L. C. Serpell and D. J. Adams, *Langmuir*, 2010, **26**, 13466–13471.

46 D. J. Adams, M. F. Butler, W. J. Frith, M. Kirkland, L. Mullen and P. Sanderson, *Soft Matter*, 2009, **5**, 1856–1862.

47 Y. Pocker and E. Green, *J. Am. Chem. Soc.*, 1973, **95**, 113–119.

48 K. A. Houton, K. L. Morris, L. Chen, M. Schmidtmann, J. T. A. Jones, L. C. Serpell, G. O. Lloyd and D. J. Adams, *Langmuir*, 2012, **28**, 9797–9806.

49 A. Z. Cardoso, A. E. Alvarez Alvarez, B. N. Cattoz, P. C. Griffiths, S. M. King, W. J. Frith and D. J. Adams, *Faraday Discuss.*, 2013, **166**, 101–116.

50 V. Foderà, M. Groenning, V. Vetri, F. Librizzi, S. Spagnolo, C. Cornett, L. Olsen, M. van de Weert and M. Leone, *J. Phys. Chem. B*, 2008, **112**, 15174–15181.

51 M. D'Amico, M. G. Di Carlo, M. Groenning, V. Militello, V. Vetri and M. Leone, *J. Phys. Chem. Lett.*, 2012, **3**, 1596–1601.

52 J. Jose and K. Burgess, *Tetrahedron*, 2006, **62**, 11021–11037.

53 X.-D. Xu, B.-B. Lin, J. Feng, Y. Wang, S.-X. Cheng, X.-Z. Zhang and R.-X. Zhuo, *Macromol. Rapid Commun.*, 2012, **33**, 426–431.

54 Y. Liu, V. Javvaji, S. R. Raghavan, W. E. Bentley and G. F. Payne, *J. Agric. Food Chem.*, 2012, **60**, 8963–8967.